Elucidating fundamental governing principles of CO_2 reduction on single-atom catalysts through interpretable machine learning

Zhiheng Ji,[a] Anjie Chen,[b] Jinxin Sun,[b,c] Peng Zhou,[b] Jiarui Wang,[b] Xiaojing Yao,[a*] Li Shi[d,e*] and Xiuyun Zhang[b*]

[a]College of Physics and Hebei Advanced Thin Films Laboratory, Hebei Normal University, Shijiazhuang 050024, China

[b]College of Physics Science and Technology, Yangzhou University, Yangzhou 225002, China

[c]Department of Physics, Southeast University, Nanjing, Jiangsu 210000, China

[d]State Key Laboratory of Flexible Electronics (LoFE) & Institute of Advanced Materials (IAM), Nanjing University of Posts and Telecommunications, Nanjing 210023, China

[e]Key Laboratory of Quantum Materials and Devices of Ministry of Education, School of Physics, Southeast University, Nanjing 21189, China

*Email: xjyao@hebtu.edu.cn, iamlshi@njupt.edu.cn, xyzhang@yzu.edu.cn

Computational details

The binding energy (E_b) was calculated to evaluate the binding strength between the $V_{B/C}$-N_n-BC_2 and TM atoms, which is defined as

$$E_b = E_{TM@V_{B/C}\text{-}N_n\text{-}BC_2} - E_{V_{B/C}\text{-}N_n\text{-}BC_2} - E_{TM} \quad (1)$$

where $E_{TM@V_{B/C}\text{-}N_n\text{-}BC_2}$, $E_{V_{B/C}\text{-}N_n\text{-}BC_2}$ and E_{TM} represent the total energies of TM@$V_{B/C}$-N_n-BC_2, $V_{B/C}$-N_n-BC_2, and the isolated TM atom.[1,2] And the cohesive energy (E_c) was calculated to represent the stability of metal atoms, which is defined as

$$E_c = \frac{E_{TMbluk}}{n} - E_{TMsingle} \quad (2)$$

where $E_{TM\ single}$, $E_{TM\ bluk}$ and n represent the energy of the isolated TM atom in vacuum, the energy of a bulk metal, and the number of atoms in the bulk crystal of TM respectively. Stabilization energy (ΔE) is a widely used energetic descriptor to evaluate the thermodynamic stability of single-atom catalysts (SACs).[3] It is typically defined as the difference between the binding energy (E_b) of a single metal atom anchored on the support and the cohesive energy (E_c) of the corresponding bulk metal:

$$\Delta E = E_b - E_c$$

To evaluate the CO_2RR activity of all the TM@$V_{B/C}$_N_n_BC_2 catalysts, the reaction free energy (ΔG) for each fundamental step was calculated according to the computational hydrogen electrode (CHE) model.[4] The change in free energy for each step can be evaluated as

$$\Delta G = \Delta E + \Delta ZPE - T\Delta S + eU + \Delta G_{pH} \quad (3)$$

where ΔE, ΔZPE, T and ΔS are the reaction energy, zero-point energy, temperature (298.15K) and entropy change, respectively. eU is the free energy contribution related to the applied potential U. ΔG_{pH} is the free energy correction of pH, which is the free energy correction related to H^+ concentration and can be calculated by $\Delta G_{pH} = k_B T \times pH \times \ln 10$, and the pH value is assumed to be 0. In the CHE framework, the potential determining step (PDS) is the elementary step with the most positive free energy change (ΔG_{max}).[5] Thus, the limiting potential (U_L) was determined by PDS calculations using

$$U_L = -\frac{\Delta G_{max}}{e} \tag{4}$$

Table S1. Comparison of representative CO_2RR catalysts reported in recent literature and those identified in this work.

Catalyst	Catalyst type	Main product	U_L (V)	Key feature / remark
Mo-I	O-coordinated SAC on doped graphene	HCOOH	-0.05	FDH-like behavior; ML-assisted DFT screening
Fe-VI	O-coordinated SAC on doped graphene	CO	-0.06	CODH-like behavior; high CO selectivity
FeN_3B	M-N_xB SAC	C_2H_4	-0.66	Orbital-symmetry-driven CO-CO coupling
Mo_2TaC_2	Double-TM MXene	CH_3OH C_2H_5OH	-0.35 -0.32	Comparable activity Toward C_1 and C_2 products
Fe-Mo_2TiC_2	TM-doped MXene	CO_2 activation (C_1)	-	Strong charge transfer and TM-CO_2 bonding
BeSi-TCNQ	Metal-free hetero-biatomic catalyst	CH_3OH	-0.29	Lowest U_L among biatomic TCNQ systems
Co@V_B-N_2-BC_2	B,N-coordinated SAC	CH_4	-0.36	Balanced intermediate binding; suppressed *OH poisoning
Fe@V_B-N_2-BC_2	B,N-coordinated SAC	CH_4	-0.35	Slightly stronger *CO_2/*HCOO stabilization

Table S2 Comparison of representative descriptor frameworks for CO_2RR activity modeling.

Category	Representative Descriptor	Typical Catalyst Systems	Prediction Scope	Transferability	Interpretability	Representative Accuracy
Electronic-structure based	*d*-band center, ICOHP	TM@h-BN, metal surfaces	CO_2 adsorption/ activation	Limited (structure-dependent)	High	Qualitative trends; $U_L \approx$ -0.52 V
Scaling-relation based	Adsorption-energy linear scaling, BEP relations	Fe-N-C, metal surfaces	Onset potential, barriers	Moderate	High	R^2 up to 0.99 (single-reaction step)
Electrochemical interface based	Surface charge, PZC	Cu-based electrodes	Activity/selectivity trends	Moderate	High	Trend-consistent with experiments
Machine-learning assisted	XGBoost, CNN+ physicochemical features	SACs, alloy surfaces	Adsorption energies	Moderate–High (data-dependent)	Moderate	$R^2 \approx$ 0.91-0.96, MAE ≈ 0.06-0.14 eV
This work	Atomic intrinsic descriptors (φ_1–φ_6)	TM@BCN SACs	Multi-step CO_2RR thermodynamics	High (structure-independent)	High (physically interpretable)	R^2 = 0.82-0.87

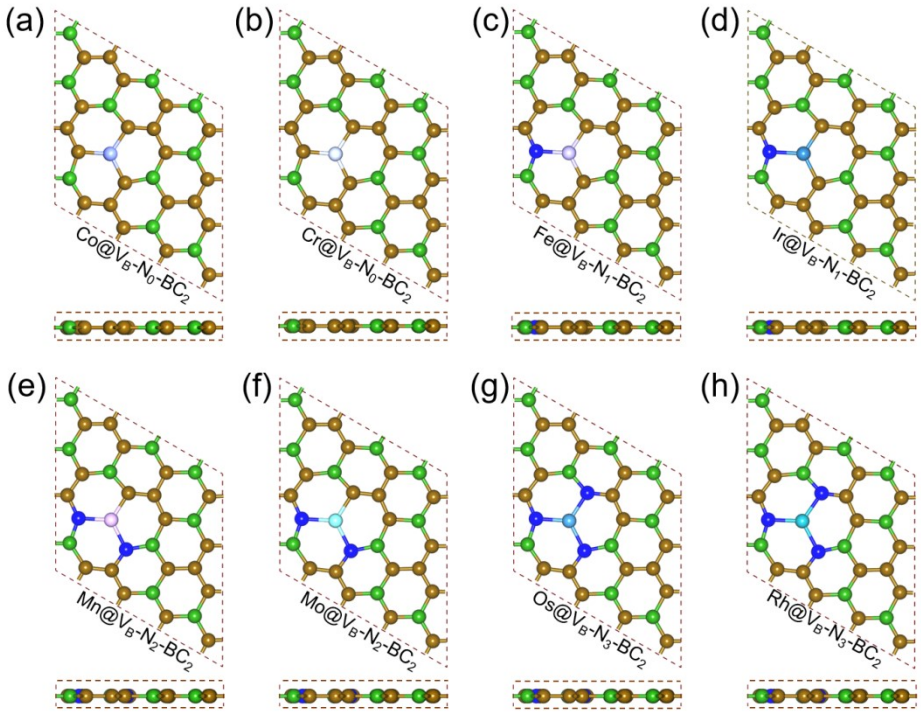

Fig. S1 Top and side views of the completely relaxed optimization of TM load on B vacancy (V_B).

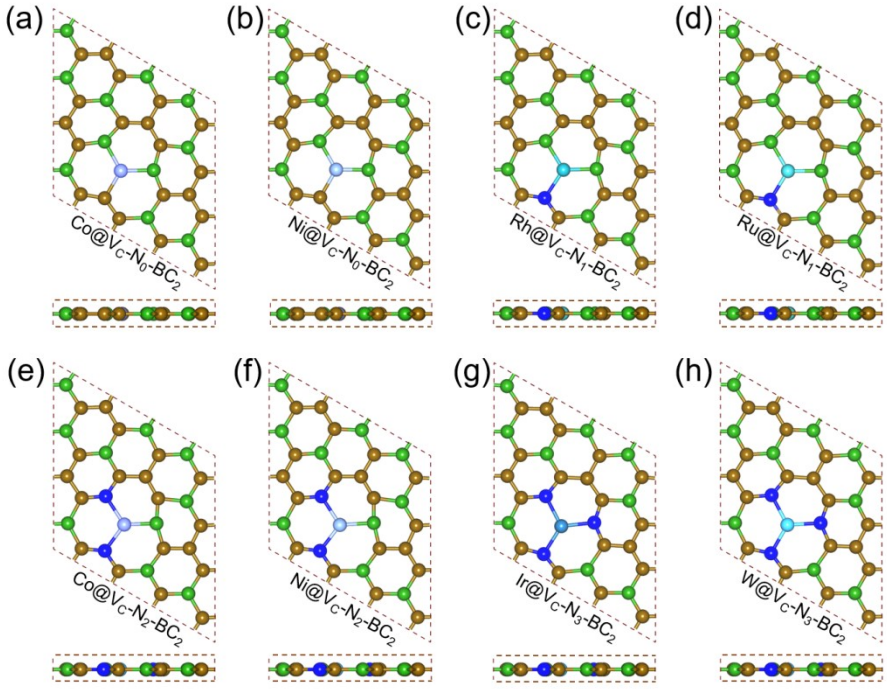

Fig. S2 Top and side views of the completely relaxed optimization of TM load on C vacancy (V_C).

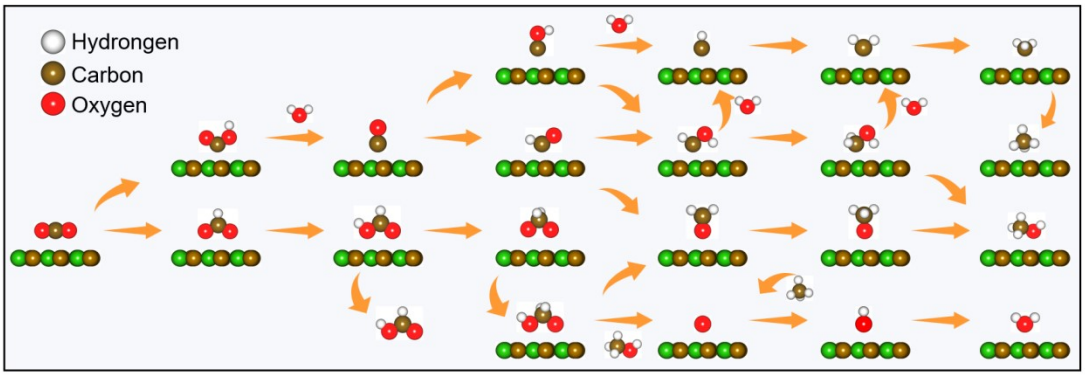

Fig. S3 Schematic diagram of possible reaction pathways for CO_2RR on $TM@V_{B/C}\_N_n\_BC_2$.

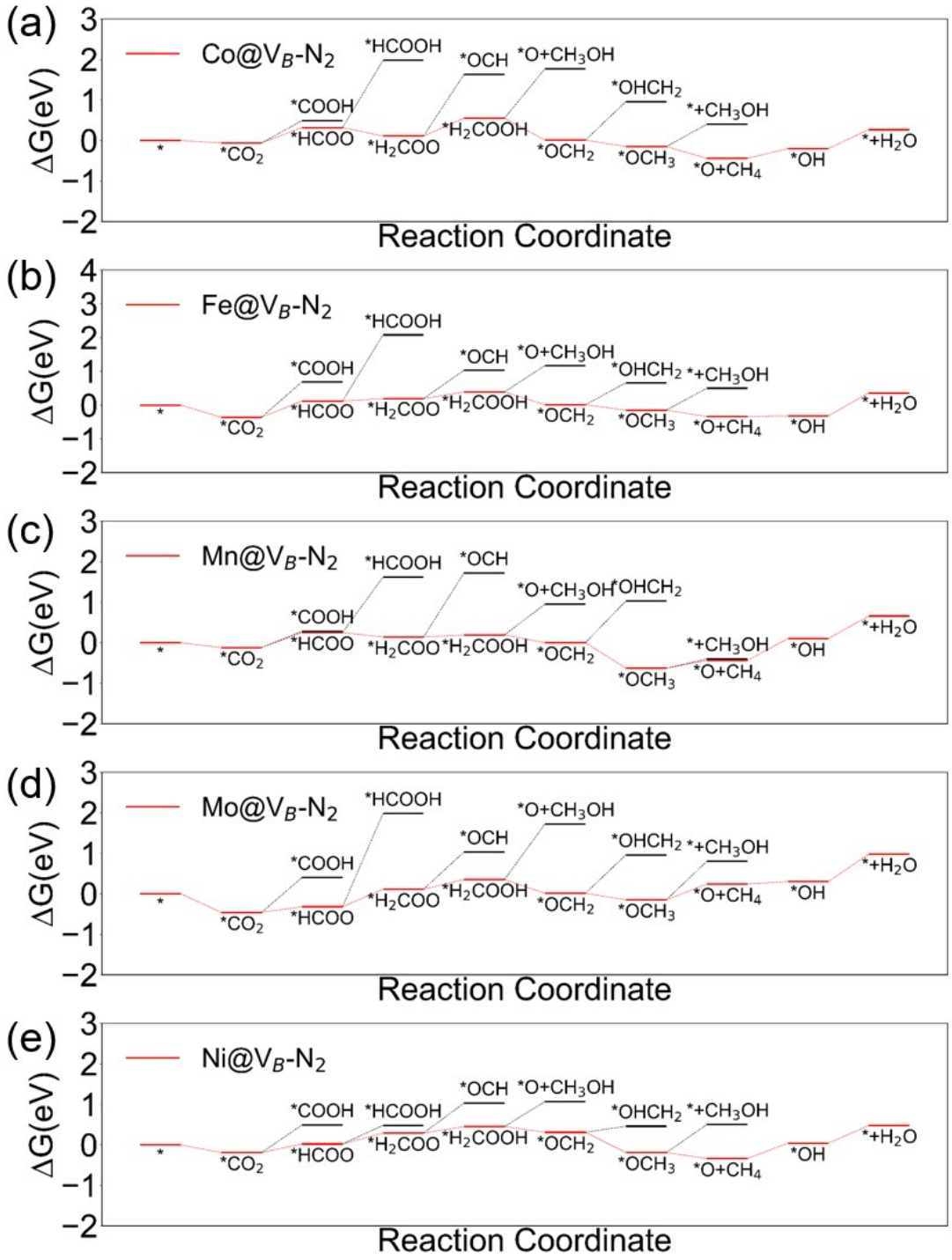

Fig. S4 Gibbs free energy ladder diagram of 5 qualified catalysts screened by high-throughput.

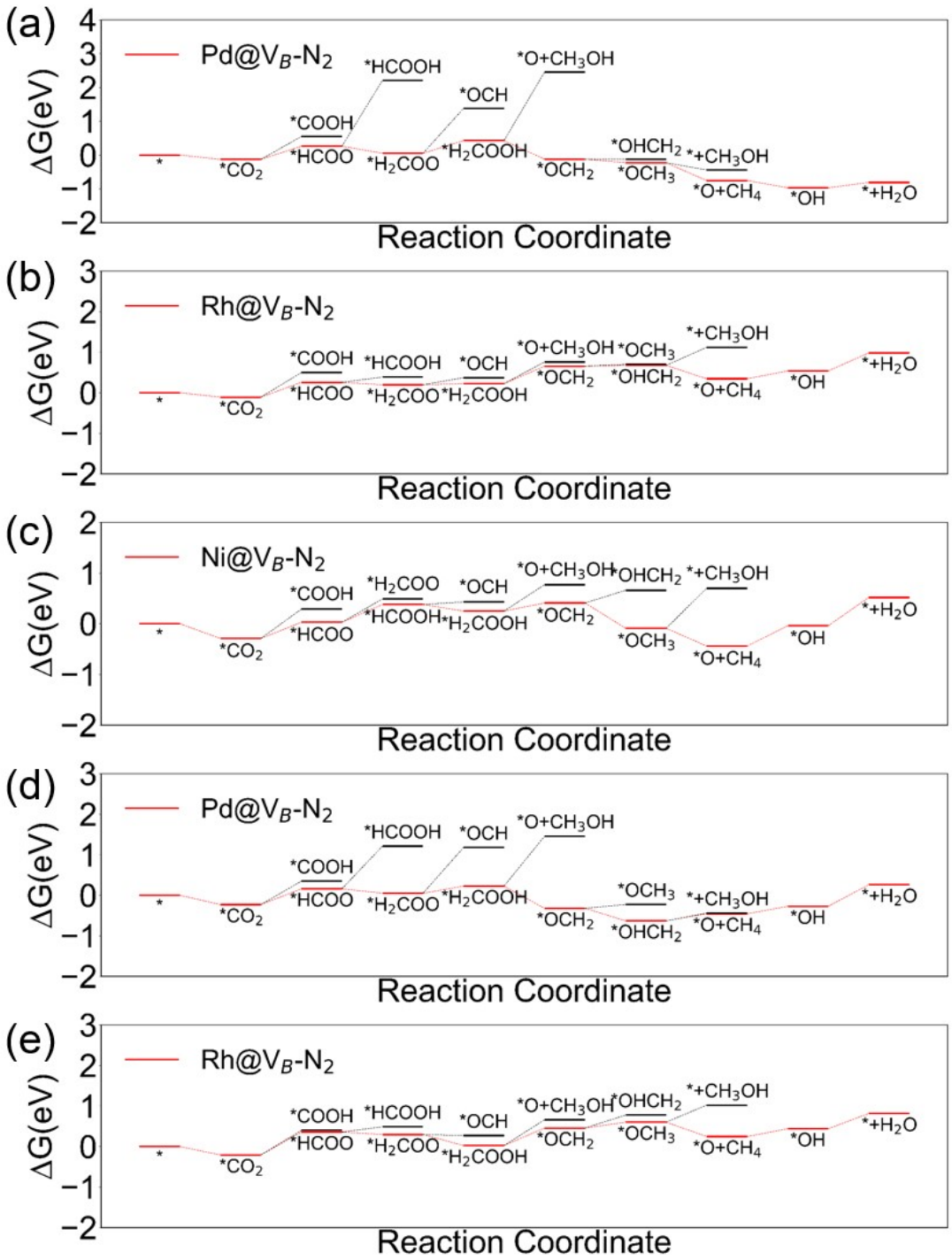

Fig. S5 Gibbs free energy ladder diagram of 5 qualified catalysts screened by high-throughput.

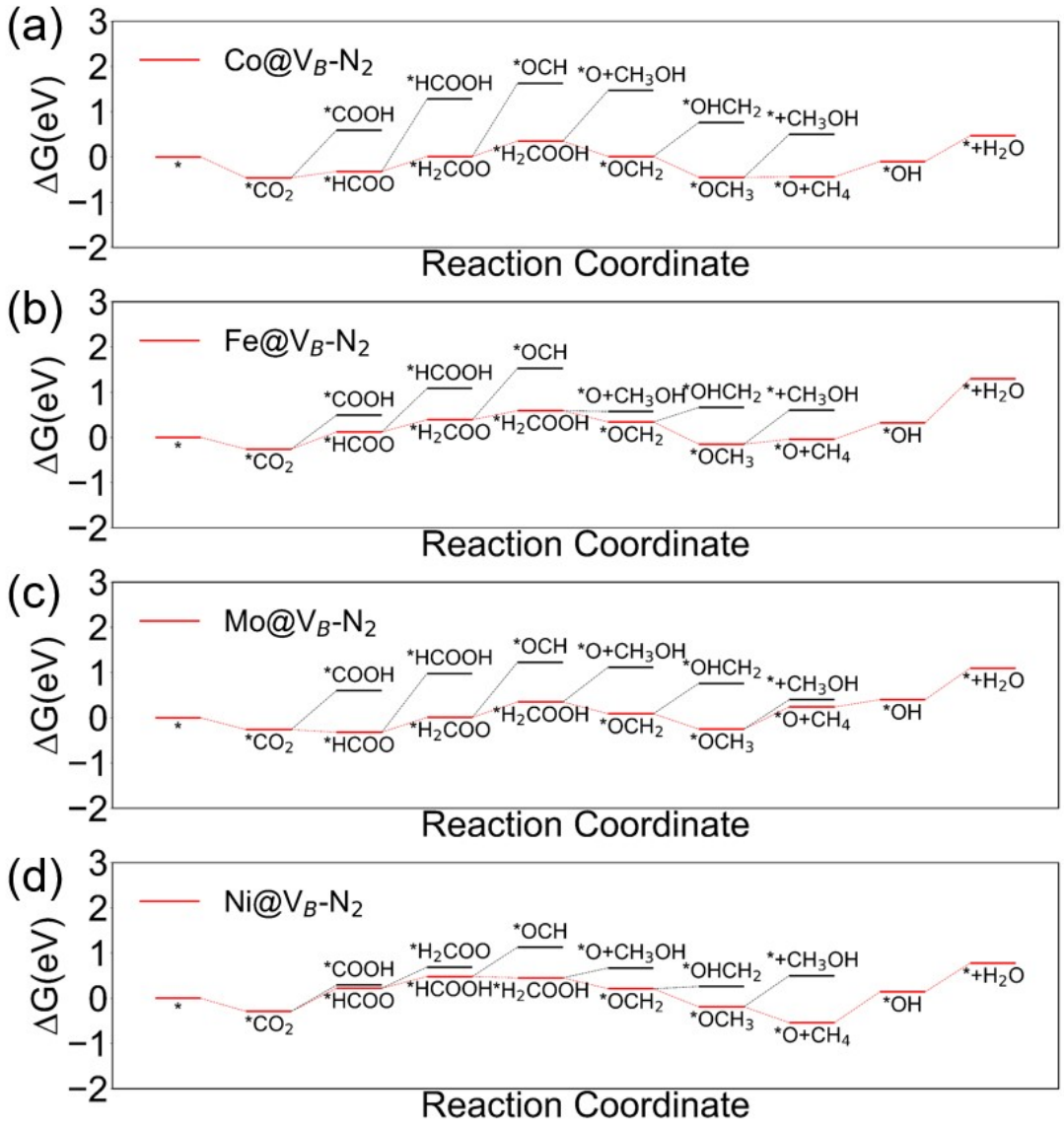

Fig. S6 Gibbs free energy ladder diagram of 4 qualified catalysts screened by high-throughput.

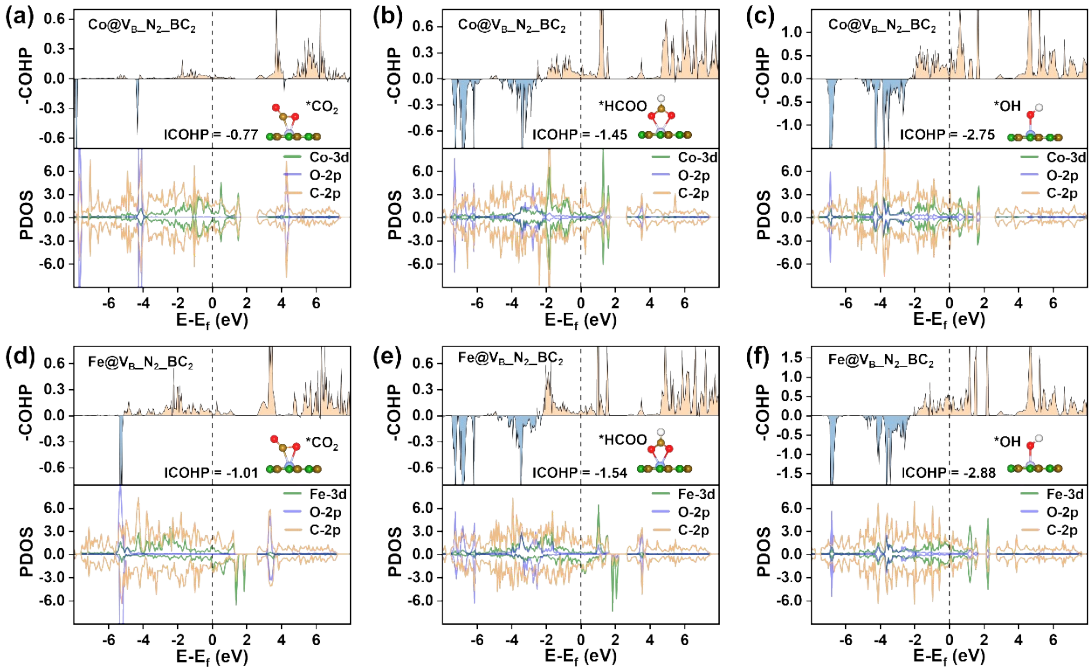

Fig. S7 (a-c) COHP and PDOS of $\Delta G(*CO_2)$, $\Delta G(*CO_2 \rightarrow *HCOO)$ and $\Delta G(*OH \rightarrow H_2O)$ on $Co@V_B\_N_2\_BC_2$; (d-f) the corresponding results for the same intermediates on $Fe@V_B\_N_2\_BC_2$. The dashed line denotes the Fermi level. The integrated crystal orbital Hamilton population (ICOHP) is used to quantitatively characterize the metal-adsorbate bonding strength, while the PDOS reveals the hybridization between the metal 3d states and the C/O 2p orbitals of the adsorbates.

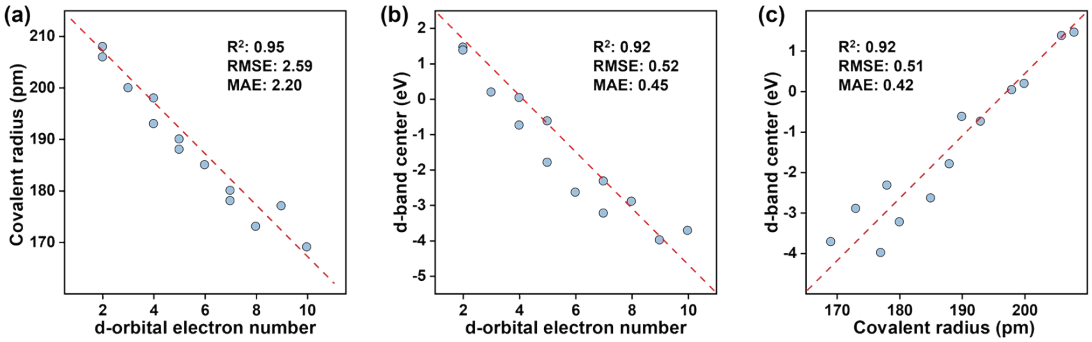

Fig. S8 (a-c) show the fitted scatter plots illustrating the intrinsic correlations between the d-orbital electron count of transition metals, their covalent radius, and the d-band center, respectively.

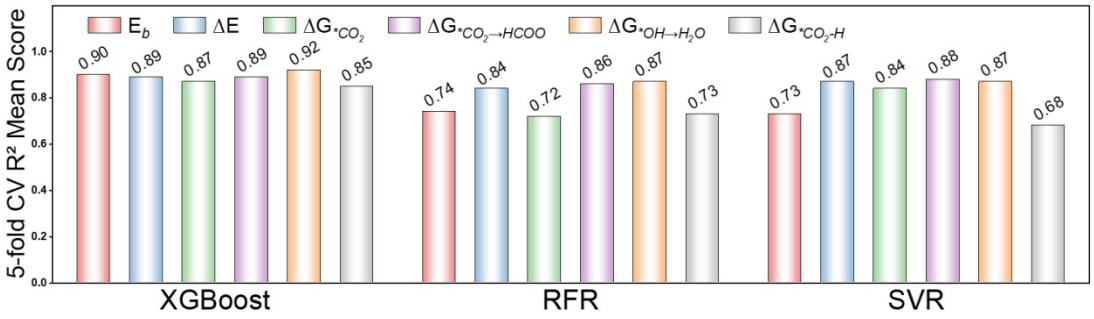

Fig. S9 Mean R^2 scores of three machine learning models using 5-fold cross-validation.

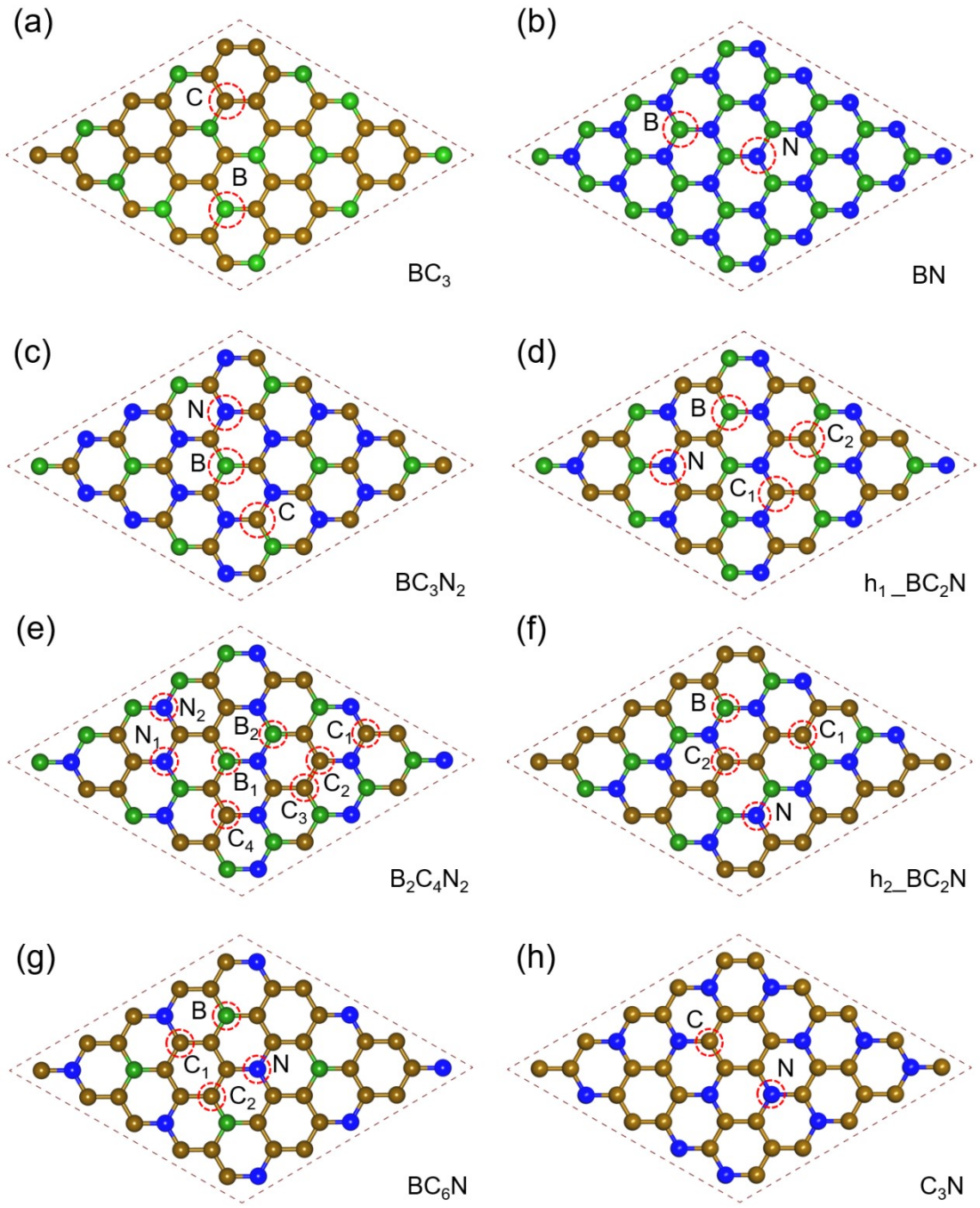

Fig. S10 The predicted structures are BC_3, BN, BC_3N_2, h_1_BC_2N, $B_2C_4N_2$, h_2_BC_2N, BC_6N and C_3N.

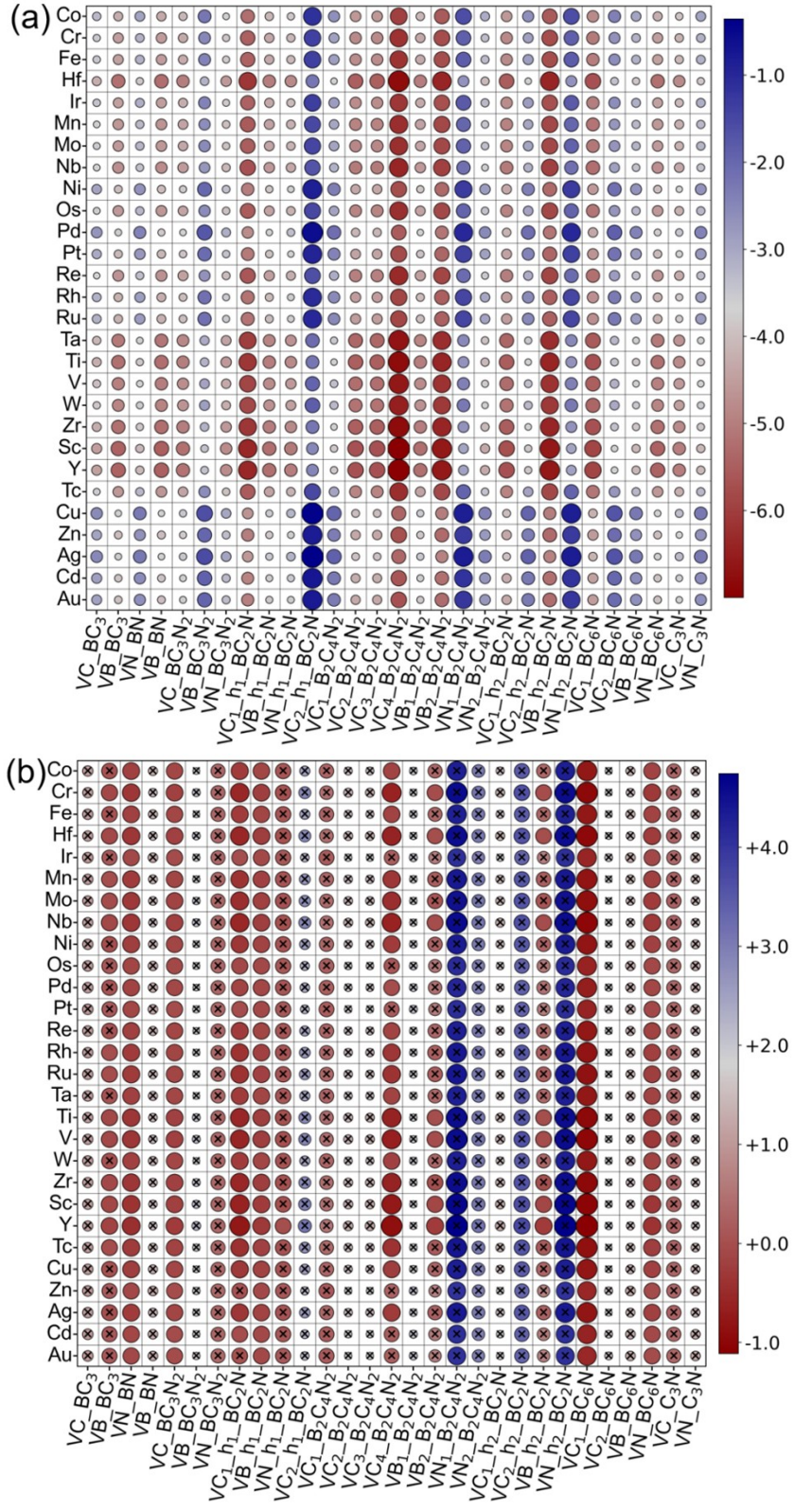

Fig. S11 Heatmap of predicted E_b and ΔE descriptor values for eight systems with graphitic structures.

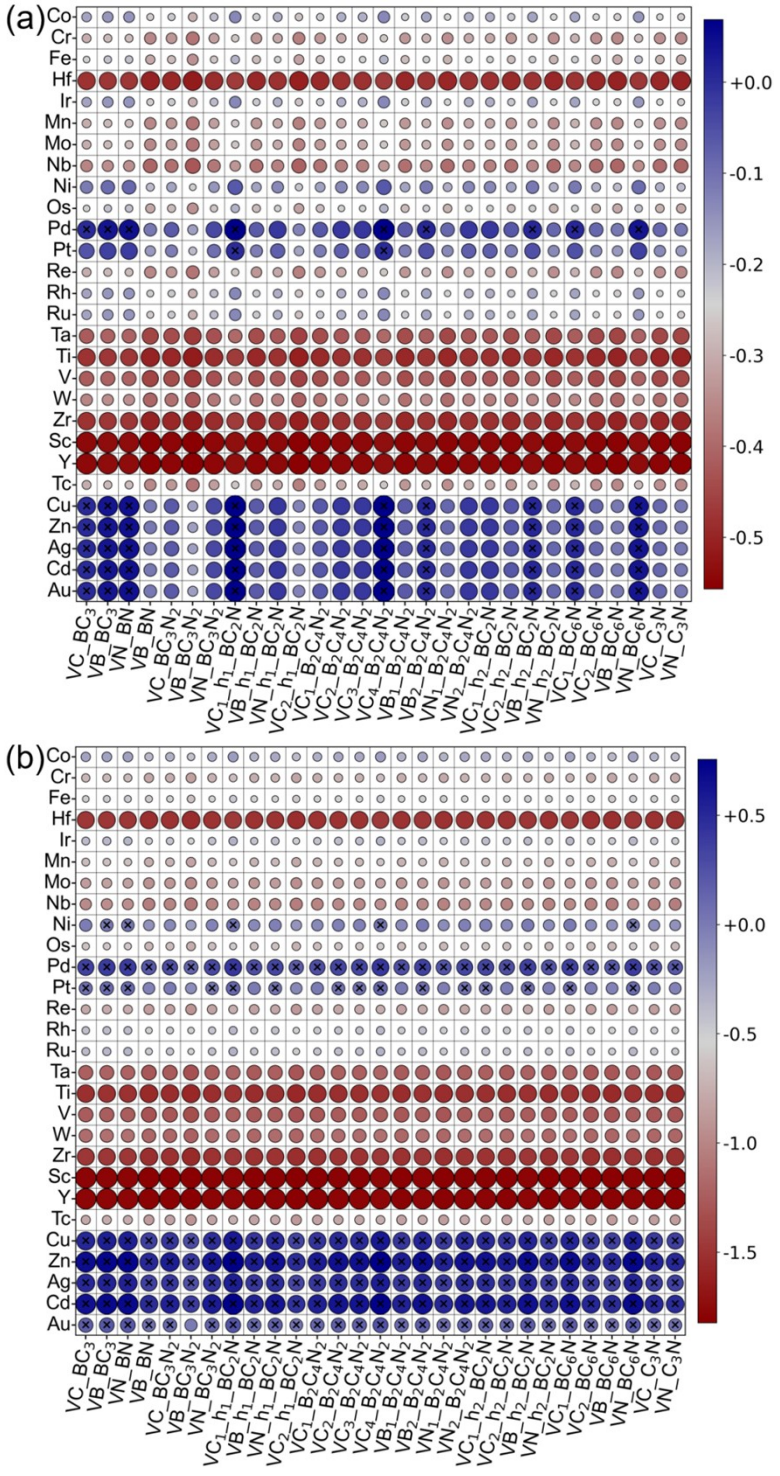

Fig. S12 Heatmap of predicted ΔG(*CO_2) and ΔG(*CO_2→*HCOO) descriptor values for eight systems with graphitic structures.

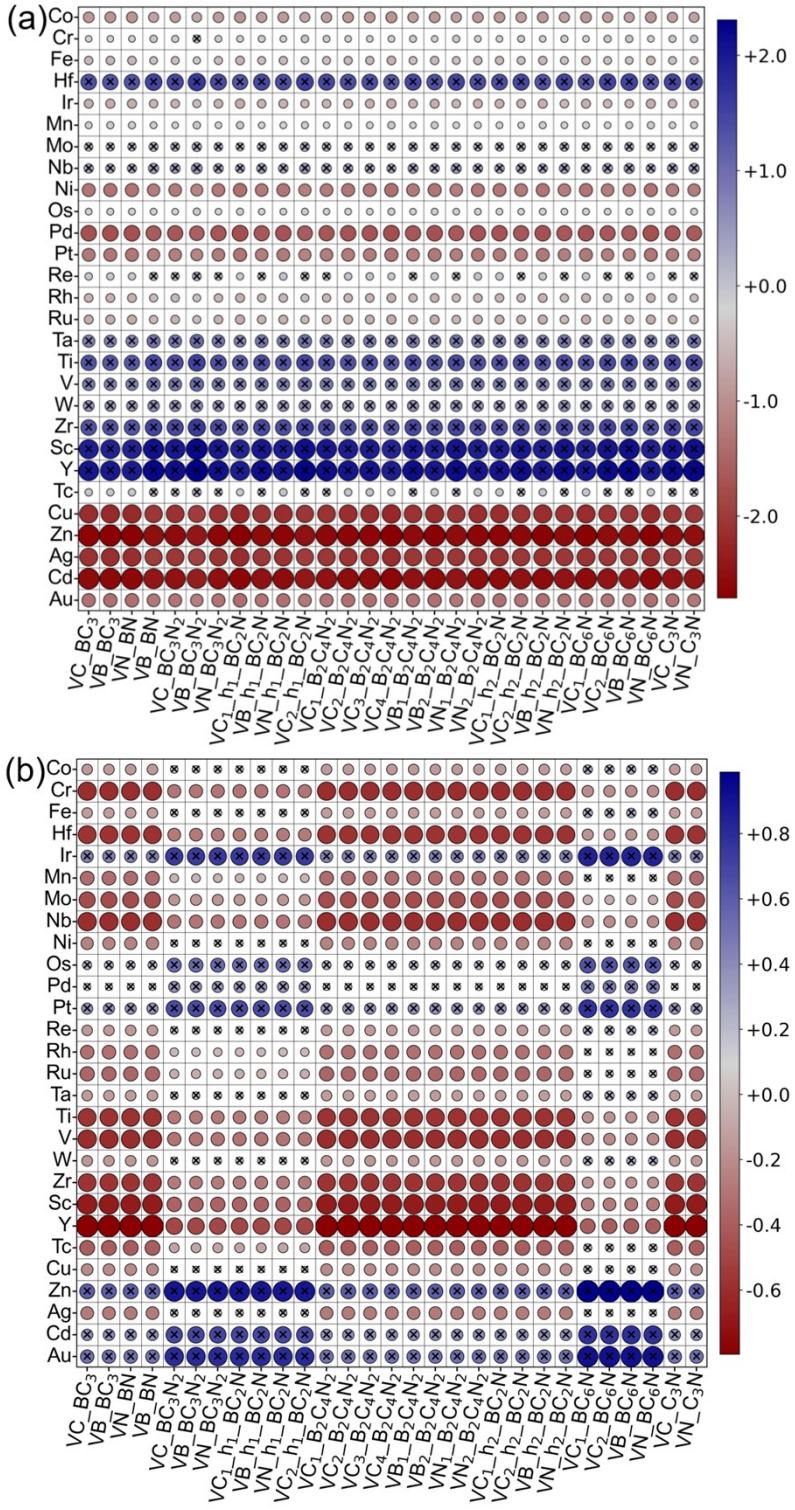

Fig. S13 Heatmap of predicted ΔG(*OH→H_2O) and ΔG(*CO_2-*H) descriptor values for eight systems with graphitic structures.

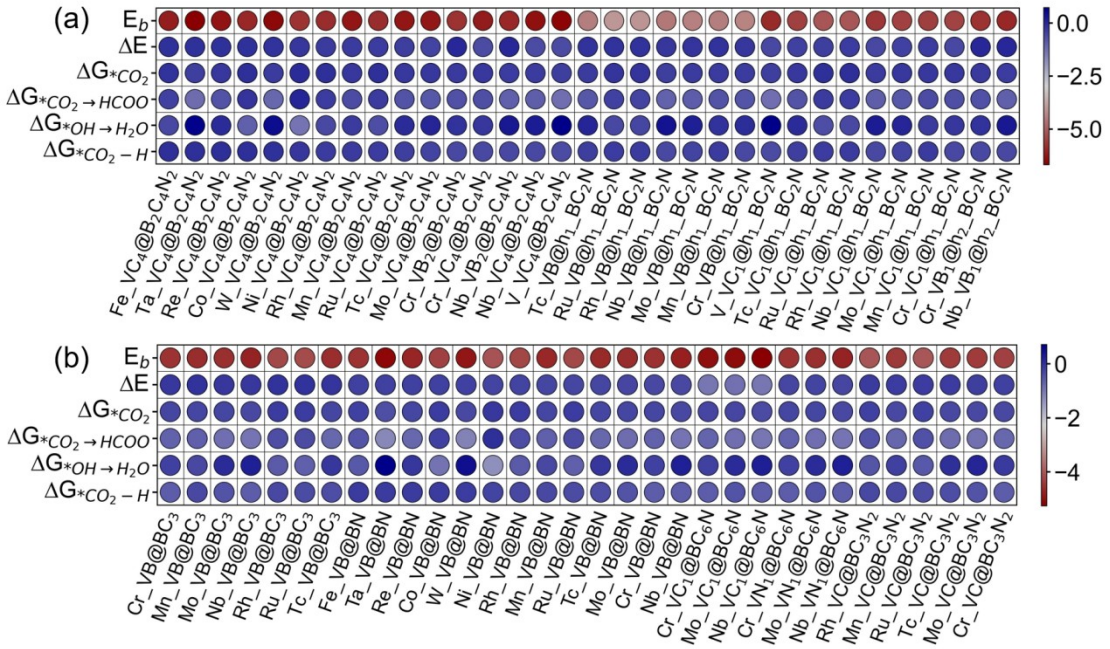

Fig. S14 Corresponding predicted values of the six descriptors for the 66 screened catalysts that satisfy all selection criteria.

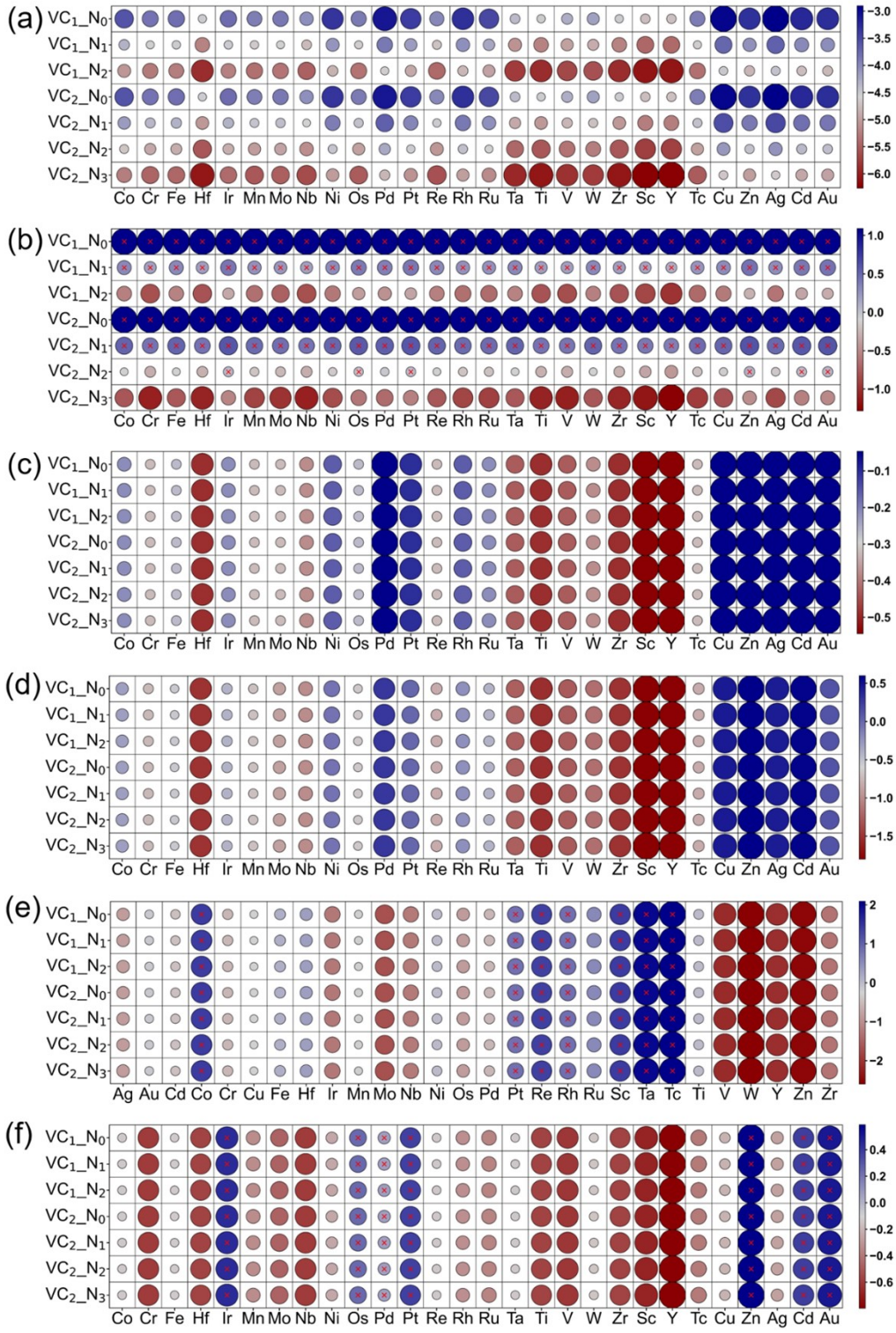

Fig. S15 Heatmap of predicted values for the descriptors E_b, ΔE, $\Delta G(*CO_2)$, $\Delta G(*CO_2 \rightarrow *HCOO)$, $\Delta G(*OH \rightarrow H_2O)$ and ΔG ($*CO_2$-*H) of graphene single-atom catalysts.

References

1 C. X. Huang, G. Li, L. M. Yang and E. Ganz, *ACS Appl. Mater. Interfaces*, 2021, **13**, 608-621.

2 L. Chen, Q. Wang, H. Gong and M. Xue, *Appl. Surf. Sci.*, 2021, **546**, 149131.

3 Y.-Q. Su, L. Zhang, Y. Wang, J.-X. Liu, V. Muravev, K. Alexopoulos, I. A. W. Filot, D. G. Vlachos and E. J. M. Hensen, *npj Computational Materials*, 2020, **6**, 144.

4 Z. Xue, X. Zhang, J. Qin and R. Liu, *Nano Energy*, 2021, **80**, 105527.

5 C.-X. Huang, S.-Y. Lv, C. Li, B. Peng, G. Li and L.-M. Yang, *Nano Res.*, 2022, **15**, 4039-4047.